Accepted manuscript of: Adrian Bekasiewicz, Khadijeh Askaripour, "Performance Comparison of Automatically Generated Topologically Agnostic Patch Antennas", 2024 25th International Microwave and Radar Conference (MIKON), doi: 10.23919/MIKON60251.2024.10633953.

Performance Comparison of Automatically Generated Topologically Agnostic Patch Antennas

Adrian Bekasiewicz
Faculty of Electronics Telecommunications and Informatics
Gdansk University of Technology
Gdansk, Poland
bekasiewicz@ru.is

Khadijeh Askaripour
Faculty of Electronics Telecommunications and Informatics
Gdansk University of Technology
Gdansk, Poland
khadijeh.askaripour@pg.edu.pl

***Abstract*—Real-world antenna design typically relies on empirical methods, where the development starts with structure synthesis followed by its iterative adjustments to achieve the desired performance. Although the outlined approach proved to be successful, it is also dependent on engineering experience. Alternatively, development can be performed automatically based on the specifications. In this work, an unsupervised design of topologically agnostic patch antennas is considered. The method involves a random generation of feasible topologies, followed by classification of the designs and their cost-efficient numerical optimization. The outlined framework has been used to determine two sets of geometrically distinct radiators dedicated to work for the frequency ranges of 5.3-5.9 GHz and 7-8 GHz, respectively. The generated antennas have been compared in terms of the electrical and radiation performances. The results indicate that the use of free-form topologies has a notable effect on the performance of antennas developed to operate in the given frequency spectrum.**

Keywords— antenna design, trust region, topology-agnostic antenna, automatic design, numerical optimization

I. Introduction

Stringent requirements concerning access to wireless medium stimulate the development of high performance, low cost, and light weight antenna geometries. Conventionally, radiators are manually, or semi-manually adjusted. The process involves synthesis of topology, followed by its modifications and tuning [1]. Despite proved usefulness, the outlined process is subject to engineering bias that stems from its human-in-the-loop nature [2], [3]. From this perspective, automatic design approaches that neglect engineering insight in favor of specification-oriented topology development seem to be an interesting alternative. In such a setup, the geometry is often obtained as a result of numerical optimization performed using population-based algorithms [7]-[12]. Unfortunately, due to the high cost of electromagnetic (EM) simulations, automatic development of radiators using conventional methods is numerically impractical unless applied to low-dimensional structures [4], [5], [6], [7].

Unsupervised design of radiators is subject to availability of EM simulation models capable of representing diverse topologies that are not limited to specific shapes [8], [9], [10]. The geometries can be specified in the form of, e.g., matrix or coordinate points. The former involves the generation of the topology from the interconnected dummy components (e.g., rectangles, or voxels) located on a predefined grid [11]. Activation, or deactivation of each element is controlled based on the contents of the matrix. Additional floating-point parameters can be used to adjust the size of the antenna under design (and hence its building blocks). The discussed representation proved to be useful for the development of pixelated or reconfigurable antennas [11]. Point-based topologies are represented as coordinates interconnected using line sections, or splines [2], [9]. This makes them scalable in terms of problem dimensionality but also convenient for optimization using conventional algorithms [12]. The main bottlenecks of both strategies include difficulties in generation of useful initial designs, as well as a large number of parameters required to ensure diverse (and hence potentially useful) topologies [9], [13], [14].

The cost of automatic antenna development can be reduced using gradient-based methods embedded into a trust region (TR) framework [15]. The algorithm proved to be useful for design of advanced radiators [15], [16], [17]. TR belongs to the class of surrogate-assisted techniques which represent a computationally viable choice for antenna optimization [16]. It is worth noting, however, that the local character of the outlined method makes it of little to no use for tuning the arbitrarily selected topologies. Consequently, for reliable and low-cost design, optimization has to be coupled with a suitable design selection strategy. A possible solution to the problem involves random generation of shapes followed by their evaluation using an appropriately defined classifier. The outlined scheme seems applicable for one-shot design of antennas. However, given the free-form nature of randomly generated topologies, one can expect that the specific performance requirements (even unconventional ones) can be fulfilled by a set of diverse, automatically determined geometries.

In this work, an automatic design of planar antennas represented in the form of coordinate points has been considered. The method involves the generation of random (yet feasible) topologies followed by their screening w.r.t. the desired electrical properties—using an appropriately defined classifier—and local optimization using the gradient-based algorithm embedded in a TR framework. The antenna used for experiments is a patch fed through a coaxial probe. The structure is represented using over 50 design parameters (that represent the radiator and location of the feed) to ensure high flexibility in terms of attainable topologies. The design problem involves the development of bandwidth-enhanced antennas dedicated to operate in frequency ranges from 5.3 GHz to 5.9 GHz and from 7 GHz to 8 GHz, respectively. The design process has been re-set to obtain two sets of antennas (3-elements each) that fulfill the requirements. Furthermore, the optimized topologies have been compared in terms of performance.

II. Antenna Structure

A free-form simulation model is required to enable the automatic, specification-oriented generation of topologies. The generic antenna structure is shown in Fig. 1. The radiator consists of a patch implemented on a dielectric substrate (ε_r = 2.55 and h = 1.524 mm), which is fed through a concentric probe. The structure resembles a conventional

This work was supported in part by the National Science Center of Poland Grant 2021/43/B/ST7/01856.

patch topology except for the radiator which is defined based on the set of coordinate points. The vector of antenna parameters is $\boldsymbol{x} = [C\ \rho_f\ \varphi_f\ \boldsymbol{\rho}\ \boldsymbol{\varphi}]^T$. To maintain geometrical feasibility, the design parameters of the radiator are defined in a cylindrical coordinate system. The variable C (in mm) scales the elements of the $\boldsymbol{x}$ vector, whereas parameters ρ_f and φ_f represent radial and angular coordinates of the probe (cf. Fig. 1). Similarly, the vectors $\boldsymbol{\rho} = [\rho_1\ \rho_2\ \ldots\ \rho_l]^T$ and $\boldsymbol{\varphi} = [\varphi_1\ \varphi_2\ \ldots\ \varphi_l]^T$ contain the radial and angular coordinates of $l = 1, \ldots, L$ interconnected points that represent the patch. The dimensions $o = 5$ mm, $r_1 = 0.615$ and $r_2 = 1.415$ mm are set constant. The parameter $A = B = 2(C{\cdot}\max(\boldsymbol{\rho}) + o)$ represents the length of substrate edge.

The EM model of the antenna (implemented in CST Studio) is dynamically generated to ensure structural flexibility while ensuring consistency and error handling. The feasibility of the antenna topology is bounded within the following lower and upper bounds $\boldsymbol{l_b} = [25\ 0\ \varphi_{0.l}\ 0.1\boldsymbol{I}\ 0.01\boldsymbol{I}]^T$ and $\boldsymbol{u_b} = [35\ \rho_{0.f}\ \varphi_{0.h}\ 0.9\boldsymbol{I}\ 0.8\boldsymbol{I}]^T$, where $\rho_{0.f} = \max(\boldsymbol{\rho}^{(0)})$, $\varphi_{0.l} = \varphi^{(0)} - \pi$, $\varphi_{0.h} = \varphi^{(0)} + \pi$; $\boldsymbol{I}$ is an L-dimensional vector of ones, and superscript (0) stands for the initial design. Note that $\boldsymbol{x}$ contains a total of $2L + 3$ elements.

III. Design Method

A. Problem Formulation

Let $\boldsymbol{R}(\boldsymbol{x})$ represent the return loss response of the antenna under design obtained for the vector $\boldsymbol{x}$ over the frequency sweep of interest. The design problem is given as:

$$\boldsymbol{x}^* = \arg\min_{\boldsymbol{x}\in\boldsymbol{X}} \left(U\left(\boldsymbol{R}(\boldsymbol{x})\right)\right) \tag{1}$$

where U is a scalar objective function and $\boldsymbol{x}^*$ represents the optimal design (specified in the feasible region of the search space $\boldsymbol{X}$) to be found. To solve the task (1) in a local optimization regime, a promising initial design is required. Here, the problem is addressed using a two-step process concerning automatic generation of random designs followed by optimization of the promising candidates.

B. Generation of Initial Designs

The promising initial designs are identified based on evaluation of randomly generated candidate designs $\boldsymbol{x}_r$ using the following classifier:

$$E = E_t + U\left(\boldsymbol{R}(\boldsymbol{x}_r)\right) \tag{2}$$

The design objective in (2) is defined as:

$$U\left(\boldsymbol{R}(\boldsymbol{x})\right) = \max\left\{\boldsymbol{R}(\boldsymbol{x})\right\}_{f_l \le f \le f_h} \tag{3}$$

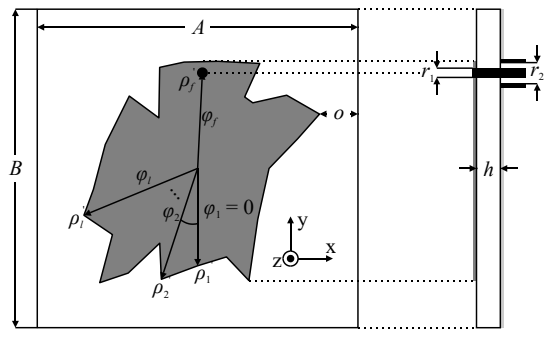

Fig. 1. Antenna topology considered for optimization with highlight on design parameters. Note that the number of ρ_l and φ_l variables is adjustable.

where f represents the frequency sweep of interest specified within the f_l to f_h interval; E_t denotes the threshold on the acceptable in-band return loss. The design generation routine is as follows.

1. Set E_t, f_l, and f_h;
2. Generate the candidate $\boldsymbol{x}_r$ and evaluate it using (2);
3. If $E < 0$, set $\boldsymbol{x}^{(0)} = \boldsymbol{x}_r$ and END; otherwise go to Step 2.

Upon identification, the initial design $\boldsymbol{x}^{(0)}$ is then optimized using the TR algorithm discussed below.

C. Optimization Algorithm

Optimization of multi-dimensional structures using conventional methods is impractical due to a large number of EM simulations required for the algorithm to converge. Here, the problem is mitigated using a gradient-based method embedded in a trust-region (TR) framework which gradually approximates $\boldsymbol{x}^*$. The TR-based design task is given as:

$$\boldsymbol{x}^{(j+1)} = \arg\min_{\left\|\boldsymbol{x}-\boldsymbol{x}^{(j)}\right\| \le \delta} \left(U\left(\boldsymbol{G}^{(j)}(\boldsymbol{x})\right)\right) \tag{4}$$

Here, $j = 1, 2, \ldots$, and δ stands for the TR radius. A model that approximates the objective function is given as:

$$\boldsymbol{G}^{(j)}(\boldsymbol{x}) = \boldsymbol{R}\left(\boldsymbol{x}^{(j)}\right) + \boldsymbol{J}\left(\boldsymbol{x}^{(j)}\right)\left(\boldsymbol{x} - \boldsymbol{x}^{(j)}\right) \tag{5}$$

where the Jacobian $\boldsymbol{J}$ is determined based on a large-step finite differentiation [19]. The algorithm is terminated when $\delta^{(j+1)} < \varepsilon$ (here, $\varepsilon = 10^{-2}$), $||\boldsymbol{x}^{(j+1)} - \boldsymbol{x}^{(j)}|| < \varepsilon$, or $||U(\boldsymbol{R}(\boldsymbol{x}^{(j+1)})) - U(\boldsymbol{R}(\boldsymbol{x}^{(j)}))|| < \varepsilon$. The TR radius is updated based on a set of standard rules. More details on the TR-based design can be found in [13], [15], [16].

IV. Results and Discussion

Two case studies that involve automatic development of bandwidth-enhanced radiators have been considered. The selected frequency ranges are: (i) 5.3 GHz to 5.9 GHz and (ii) 7 GHz to 8 GHz, respectively. For each bandwidth, three antenna designs have been optimized. The numerical results are followed by the discussion of the considered structures' performance. It is worth noting that, in the course of topology generation, the scaling coefficient is fixed to $C = 30$. The TR-based optimization is governed using the least-squares objective function:

$$U = \frac{1}{N}\sum_{n=1}^{N} \max\left(R_n(\boldsymbol{x}) - R_{\max}, 0\right)^2 \tag{6}$$

where $R_n(\boldsymbol{x}) \in \boldsymbol{R}(\boldsymbol{x})$ is the nth point of the discrete frequency response from the $f_l \le f \le f_h$ range, N is the overall number of points from f_l to f_h, and $R_{\max}$ is the return-loss threshold (here, $R_{\max} = -10$ dB is used).

A. First Case Study

The initial topology-agnostic designs have been found using the method of Section III. The threshold value in (2) has been set to $E_t = -4$ dB. The resulting starting points $\boldsymbol{x}_1^{(0)}$, $\boldsymbol{x}_2^{(0)}$, and $\boldsymbol{x}_3^{(0)}$ have been then optimized using the algorithm outlined in Section III and objective function (6). The topologies and return loss responses (at the initial and optimized designs) are given in Figs. 2 and 3, whereas Fig. 4 shows the radiation pattern responses in the yz-plane (cf. Fig. 1) at the 5.8 GHz frequency for the optimized radiators. Note that the design method of Section III is oriented towards numerical optimization of the topologies w.r.t. their electrical

performance. Hence, the radiation responses are merely a by-product of the return-loss-oriented design.

The results are in-line with the expectation that the desirable electrical performance of patch-based structures can be achieved using various topologies. One can note that the optimized first and second designs are similar in terms of geometry. At the same time, the locations of their feeds are substantially different. The obtained shapes also indicate that, for the first and third cases, the differences between initial and optimized solutions (shape-wise) are relatively subtle. However, for the second design, the final geometry represents a notable change from the starting point. The results suggest that the search space for the problem at hand is highly multimodal (which is reasonable given the high dimensionality of the simulation model), which causes premature convergence of the TR-based algorithm. This observation seems to be supported by the return loss responses shown in Fig. 3, which demonstrate that the first and third design violate (albeit slightly) the performance requirements. However, the effect might also be attributed to the nature of the obtained response as they feature only one in-band local maxima for the first and third design, whereas the second design is characterized by two maxima.

The radiation pattern characteristics indicate that the designs with narrower bandwidth produce the single-lobe responses. At the same time, a dual-lobe pattern is obtained for the second design. The gains of the optimized radiators in the directions of maximum radiation are 6.10 dBi (at 15° angle in the yz-pattern; cf. Fig. 1), 6.44 dB (40°), and 8.17 dB (3°), respectively.

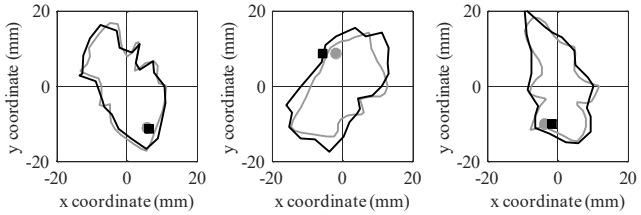

Fig. 2. Initial (gray) and optimized (black) geometries of the topology-agnostic antenna optimized for 5.3-5.9 GHz range at designs: (a) 1, (b) 2, and (c) 3.

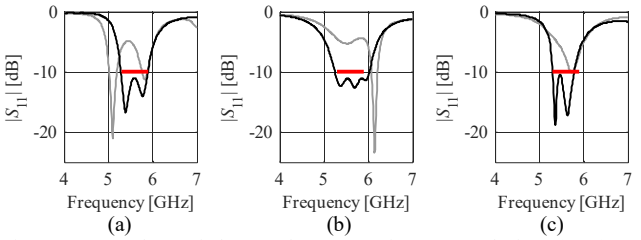

Fig. 3. Return loss of the topology-agnostic antenna before (gray) and after (black) optimization at designs: (a) 1, (b) 2, and (c) 3. The red line denotes design specification.

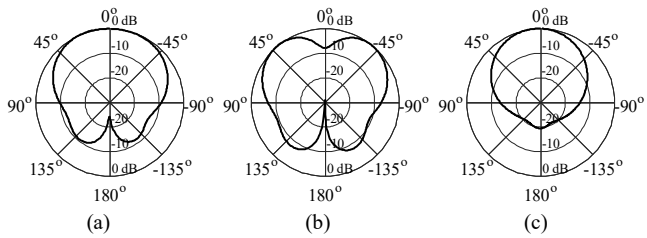

Fig. 4. Radiation patterns (yz-plane) at 5.8 GHz obtained for designs: (a) 1, (b) 2, and (c) 3. Note that the design 2 is characterized by the broadest bandwidth but also a dual-lobe radiation pattern.

B. Second Case Study

Owing to the fixed scaling coefficient, the candidate designs generated for the second case study (frequency range from 7 GHz to 8 GHz) are electrically larger compared to the ones discussed before. As a consequence, one can expect higher quality of the randomly generated designs. Having that in mind, a more aggressive threshold for the classifier, i.e., $E_t = –6.5$ dB has been selected here.

Figures 5 to 7 illustrate the geometries, as well as electrical responses and radiation pattern characteristics obtained for the selected antenna designs. As compared to the first case study, the identified topologies are less elongated and feature increased complexity (here understood in terms of convex/concave segments). It should be noted that the initial and optimized geometries are relatively similar, which (in this case) is mostly due to high-quality starting points. The obtained electrical responses demonstrate high performance of the designs, with return losses well below –10 dB for most of the operational bandwidth. Return loss responses for two of the three solutions are characterized by two local maxima within the range of interest. The radiation pattern characteristics are somewhat similar to the ones of Section IV.*A* in a sense that the structure characterized by the broadest bandwidth also features a dual-lobe radiation pattern. It is worth noting that the gains obtained for the antennas in directions of maximum radiation amount to 7.35 dB (at the 14° angle in the yz-plane; cf. Fig. 1), 2.07 dB, and 7.1 dB (–33°), respectively. Clearly, a with relatively low gain, the second design is an outlier in terms of far-field radiation performance.

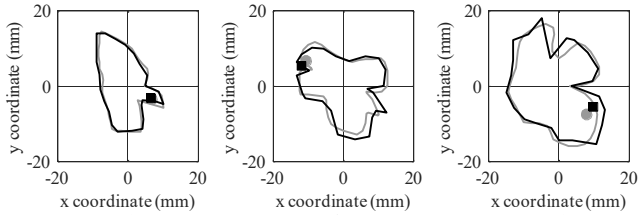

Fig. 5. Initial (gray) and optimized (black) geometries of the topology-agnostic antenna optimized for 7-8 GHz range at designs: (a) 1, (b) 2, and (c) 3.

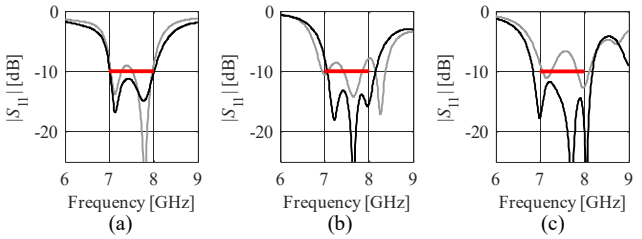

Fig. 6. Return loss of the topology-agnostic antenna before (gray) and after (black) optimizati4 7on at designs: (a) 1, (b) 2, and (c) 3. The red line denotes design specification.

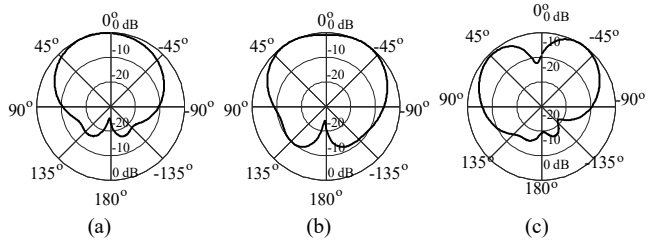

Fig. 7. Radiation patterns (yz-plane) at 7.5 GHz obtained for designs: (a) 1, (b) 2, and (c) 3. Note that the last design is characterized by a dual-lobe response, whereas design 2 features wide main lobe and a low gain.

C. Discussion

Table I provides a comparison of the developed antennas in terms of bandwidth, gain, and size. All of the structures demonstrate broadband behavior (especially when compared to the conventional patch topologies) with bandwidth ranging from 9% to as much as 18% (a two-fold change). Note that the relative bandwidth is broader for the antennas operating in the 7 GHz to 8 GHz range. This effect, however, is associated with their relatively large dimensions compared to the structures of Section IV.*A*. The maximum gains are fairly consistent for four out of six structures. A slight deterioration of gain for design 2 can be attributed to its dual-lobe behavior. As it comes to structure 5, it is a noticeable outlier in terms of radiation performance. The results indicate that automatic generation of antenna topologies should account not only for electrical but also other performance characteristics relevant w.r.t. the intended applications. The average optimization cost amounts to 203 EM simulations per design. However, due to random nature of topology synthesis, generation of suitable initial geometries required from around 500 to 2500 additional EM simulations.

Potential application scenarios for the generated structures include WiFi systems (for antennas of Section IV.*A*) as well as ultra-wideband in-door localization at eight channel of the available spectrum (for structures of Section IV.*B*). It should be noted that, dual-lobe radiation pattern comes at the expense of degraded gain (especially when compared to conventional structures). On the other hand, the somewhat unconventional dual-lobe responses obtained for antennas 2 and 6 might represent an advantage for certain use cases. The latter might include installation in challenging conditions where the gain of omnidirectional radiators is insufficient to ensure sufficient quality of service within the desired area while directional antennas do not provide sufficient coverage (e.g., in convex corners of the area monitored using an in-door localization system).

V. Conclusion

In this paper, the automatic generation and optimization of planar antenna topologies represented in the form of coordinate points have been considered. The design method has been applied to obtain a total of six radiators dedicated to work within the frequency bands from 5.3 GHz to 5.9 GHz and 7 GHz to 8 GHz, respectively. The optimized antennas can be applied as components of wireless communication and/or in-door localization systems. Despite being based on patch topology, the optimized structures offer relatively broad operational bandwidths that range from 9% to 18%, far exceeding the capabilities of conventional radiators. Two of the obtained designs feature unconventional dual-lobe radiation patterns, which have been obtained as a by-product of electrical-performance-oriented optimization.

TABLE I. A Comparison of the Optimized Antenna Designs

Design	Size	f_L	f_H	BW		Gain (dB)	
	(mm × mm)	(GHz)	(GHz)	(GHz)	(%)	5.6 GHz	5.8 GHz
1	43.4 × 43.4	5.28	5.89	0.61	11	7.37	6.10
2	44.9 × 44.9	5.25	6.02	0.77	13	5.04	6.44
3	50.6 × 50.6	5.3	5.79	0.49	9	7.85	8.17
Design	Size	f_L	f_H	BW		Gain (dB)	
	(mm × mm)	(GHz)	(GHz)	(GHz)	(%)	7.5 GHz	7.8 GHz
4	38 × 38	7.01	8.01	1	13	7.35	7.54
5	38.5×38.5	7.05	8.14	1.09	15	2.07	3.90
6	45.9×45.9	6.84	8.18	1.34	18	7.1	4.64

Further work will focus on manufacturing and measurements of the antenna prototypes, re-definition of the objective function so as to account for the electrical- and field-related performance characteristics, as well as implementation of warm-start mechanisms (i.e., database of initial designs) and embedding the design within a globalized optimization loop so as to reduce the cost of topologies generation and mitigate the risk of premature convergence.

References

[1] M. Sharma, A. K. Gautam, N. Agrawal, and N. Singh, "Design of an antipodal balanced taper-fed broadband planar antenna for future 5G and remote sensing satellite link applications," *Int. J. Electron. Commun.*, vol. 123, 2020.

[2] M.S. Khan, S.M. Asif, and R. M. Shubair, "A compact CSRR-enabled UWB diversity antenna," *IEEE Ant. Wireless Prop. Lett.*, vol. 16, pp. 808–812, 2017.

[3] Y.F. Liu, P. Wang, and H. Qin, "Compact ACS-fed UWB antenna for diversity applications," *Electronics Lett*., vol. 50, no. 19, pp. 1336–1338, 2014.

[4] S. Mirhadi, N. Komjani, and M. Soleimani, "Ultra wideband antenna design using discrete Green's functions in conjunction with binary particle swarm optimization," *IET Microwaves Ant. Prop.*, vol. 10, no. 2, pp. 184–192, 2016.

[5] A. Bekasiewicz, "Low-cost automated design of compact branch-line couplers," *Sensors*, vol. 20, art no. 3562, 2020.

[6] A. Bekasiewicz and S. Koziel, "Reliable multistage optimization of antennas for multiple performance figures in highly-dimensional parameter spaces," *IEEE Ant. Wireless Prop. Lett*., vol. 18, no. 7, pp. 1522–1526, 2019.

[7] H. Aliakbari, et al. "ANN-based design of a versatile millimetre-wave slotted patch multi-antenna configuration for 5G scenarios," *IET Microwaves Ant. Prop.*, vol. 11, no. 9, pp. 1288–1295, 2017.

[8] M. Capek, L. Jelinek, and M. Gustafsson, "Shape synthesis based on topology sensitivity," *IEEE Trans. Ant. Prop.*, vol. 67, no. 6, pp. 3889–3901, 2019.

[9] M. Ghassemi, M. Bakr, and N. Sangary, "Antenna design exploiting adjoint sensitivity-based geometry evolution," *IET Microwaves Ant. Prop.*, vol. 7, no. 4, pp 268–276, 2013.

[10] L. Lizzi, F. Viani, R. Azaro, and A. Massa, "Optimization of a spline-shaped UWB antenna by PSO," *IEEE Ant. Wireless Prop. Lett*., vol. 6, pp. 182–185, 2007.

[11] J.P. Jacobs, "Accurate modeling by convolutional neural-network regression of resonant frequencies of dual-band pixelated microstrip antenna," *IEEE Ant. Wireless Prop. Lett*., vol. 20, no. 12, pp. 2417–2421, 2021.

[12] A.D. Boursianis, et al., "Multiband patch antenna design using nature-inspired optimization method," *IEEE Open J. Ant. Prop.*, vol. 2, pp.151–162, 2020.

[13] A. Bekasiewicz, P. Kurgan, and S. Koziel, "Numerically efficient miniaturization-oriented optimization of an ultra-wideband spline-parameterized antenna," *IEEE Access*, vol. 10, pp. 21608–21618, 2022.

[14] N. Jin and Y. Rahmat-Samii, "Advances in particle swarm optimization for antenna designs: Real-number, binary, single-objective and multiobjective implementations," *IEEE Trans. Ant. Prop.*, vol. 55, no. 3, pp. 556–567, 2007.

[15] S. Koziel and A. Bekasiewicz, "Fast EM-driven size reduction of antenna structures by means of adjoint sensitivities and trust regions," *IEEE Ant. Wireless Prop. Lett*., vol. 14, pp. 1681–1684, 2015.

[16] A. Bekasiewicz, "Optimization of the hardware layer for IoT systems using a trust region method with adaptive forward finite differences," *IEEE IoT J.*, vol. 10, no. 11, pp. 9498–9512, 2023.

[17] S. Koziel and S.D. Unnsteinsson, "Expedited design closure of antennas by means of trust-region-based adaptive response scaling," *IEEE Ant. Wireless Prop. Lett*., vol. 17, no. 6, pp. 1099–1103, 2018.

[18] H. Zhai, Z. Ma, Y. Han, and C. Liang, "A compact printed antenna for triple-band WLAN/WiMAX applications," *IEEE Ant. Wireless Prop. Lett*., vol. 12, pp. 65–68, 2013.

[19] A. Pietrenko-Dabrowska and S. Koziel, *Response feature technology for high-frequency electronics: optimization, modeling, and design automation*, Springer, New York, 2023.